# Feedforward and feedback influences through distinct frequency bands between two spiking-neuron networks

Leonardo Dalla Porta [1,*] Daniel M. Castro [2,*] Mauro Copelli,[2] Pedro V. Carelli,[2,†] and Fernanda S. Matias [3,‡]

[1]*Systems Neuroscience, Institut d'Investigacions Biomèdiques August Pi i Sunyer (IDIBAPS), Barcelona 08036, Spain*
[2]*Departamento de Física, Universidade Federal de Pernambuco, Recife PE 50670-901, Brazil*
[3]*Instituto de Física, Universidade Federal de Alagoas, Maceió, Alagoas 57072-970, Brazil*

Several studies on brain signals suggested that bottom-up and top-down influences are exerted through distinct frequency bands among visual cortical areas. It was recently shown that theta and gamma rhythms subserve feedforward, whereas the feedback influence is dominated by the alpha-beta rhythm in primates. A few theoretical models for reproducing these effects have been proposed so far. Here we show that a simple but biophysically plausible two-network motif composed of spiking-neuron models and chemical synapses can exhibit feedforward and feedback influences through distinct frequency bands. Different from previous studies, this kind of model allows us to study directed influences not only at the population level, by using a proxy for the local field potential, but also at the cellular level, by using the neuronal spiking series.

## I. INTRODUCTION

Understanding the relationship between structural and functional connectivities in the brain is one of the greatest challenges of neuroscience. In other words, this means associating specific anatomical networks with different possible patterns of activity and especially with information flow. Regarding the hierarchical organization of cortical regions, several anatomical studies have shown that the structural connections from the primary sensory areas to higher-order areas (i.e., feedforward or the bottom-up direction) are reciprocated by connections in the opposite direction (known as feedback or top-down connections) [1,2]. Furthermore, many cognitive phenomena, including visual attention and perception, have been related to both feedforward and feedback influences [3,4].

In visual cortical areas of primates, the hierarchy is reflected not only in their projection patterns along with different cortical layers (anatomical connectivity) but also in relation to local rhythmic synchronization (functional connectivity). For example, feedforward projections typically originate from superficial layers, whereas feedback projections originate predominantly from infragranular layers. Synchronization in the gamma frequency band is strongest in superficial layers, whereas synchronization in the alpha-beta frequency band is strongest in infragranular layers [5–7]. Moreover, electrical stimulation of cortical area V1 induces enhanced oscillatory activity in cortical region V4 in the gamma band, whereas the stimulation of V4 induces enhanced alpha-beta-band activity in V1 [8]. Taken together, these results suggest that gamma might subserve feedforward and alpha-beta might subserve feedback information flow [9,10]

Two recent experimental studies with primates corroborated these ideas. First, it was shown through large-scale high-density electrocorticography and anatomical projection patterns in rhesus macaques that among eight visual cortical areas gamma is systematically stronger in the feedforward direction and beta is stronger in the feedback direction [11]. Second, it was reported that in human visual areas feedforward or feedback could be determined based on retrograde tracing data in homologous macaque visual areas. Moreover, by using magnetoencephalogram data and spectral Granger causality analysis to determine causal influences among cortical areas, Michalareas *et al.* [12] showed that feedforward projections were predominant in the gamma band, whereas feedback projections were predominant in the alpha-beta band.

The mechanisms underlying these frequency-specific influences are still under investigation. A large-scale network using mean-field rate models of the Wilson-Cowan type was employed to reproduce the feedforward and feedback influences through distinct frequency bands among eight selected cortical areas of interest (V1, V2, V4, DP, 8m, 8l, TEO, and 7A) [13]. Even though Mejias *et al.* [13] reproduced the Granger causality patterns observed by Bastos *et al.* [11] among the mentioned regions, a firing rate model cannot be used to study the spiking time relations between neurons in different areas, which is a natural future step of investigation in experimental studies [11]. Furthermore, spiking-neuron models allow us to investigate the effect of neuronal properties at large-scale function connectivity. For example, one could explore the functional significance of important cellular properties such as heterogeneity [14] and homeostasis [15] for the feedforward and feedback influences through distinct frequency bands, as well as their role in the underlying mechanisms promoting the phenomenon.

---

*These authors contributed equally to this work.
†pedro.carelli@ufpe.br
‡fernanda@fis.ufal.br

In this direction, Lee *et al.* [9,16] have developed a biophysically based model to show how top-down signals in the beta and gamma regimes can interact with a bottom-up gamma rhythm to provide regulation of signals between the cortical areas and among layers. However, in their studies, they were interested in reproducing *in vitro* observations between the primary auditory cortex and adjacent association cortex and did not reproduce the unidirectional gamma feedforward and unidirectional alpha-beta feedback verified in visual areas [11,12].

Here we show that two reciprocally connected cortical-like populations composed of randomly connected Izhikevich neurons can present Granger causality from 1 to 2 in the gamma band, whereas the influence from 2 to 1 occurs in the alpha band. This means that our simple model qualitatively reproduces the experimental results of feedforward and feedback influences through distinct frequency bands at the visual cortex [11,12].

In Sec. II, we describe the neuronal population model as well as the parameters that we use to change interarea coupling. We also describe the spectral time series analysis that we use to characterize influences at the two different spatial scales: populational and neuronal levels. In Sec. III, we report our results, showing that our motif can exhibit bottom-up and top-down influences in the alpha ($\sim$10 Hz) and gamma ($\sim$40 Hz) bands. One of the advantages of a spiking-neuron network model is that one can explore information measures at the neuronal level such as the directional spike-train pairs associated with directional information (DI) [17]. In fact, we employ this method and show that the spiking-neuron trains can give us complementary information about the direction of influence. Concluding remarks and a brief discussion of the significance of our findings for neuroscience are presented in Sec. IV.

## II. METHODS

### A. Modeling the spiking-neuron networks

We modeled two neuronal populations following the ideas proposed in Ref. [18]. Both populations, namely, 1 and 2, consist of 400 excitatory and 100 inhibitory neurons each. Each neuron is modeled by the Izhikevich model [19]:

$$\frac{dv}{dt} = 0.04v^2 + 5v + 140 - u + \sum I_{\text{syn}} + I_{\text{DC}} \qquad (1)$$

and

$$\frac{du}{dt} = a(bv - u). \qquad (2)$$

If $v \geqslant 30$ mV, then $v$ is reset to $c$ and $u$ to $u + d$. $v$ and $u$ stand for the membrane potential and the membrane recovery variable (activation of the $K^+$ ionic current and inactivation of the $Na^+$ ionic current), respectively. $a, b, c$, and $d$ are dimensionless parameters that account for the firing pattern heterogeneities, which are randomly distributed according to the neuron's nature. For excitatory neurons $a = 0.02$, $b = 0.20$, $c = -65 + 15\sigma^2$, and $d = 8 - 6\sigma^2$, whereas for inhibitory neurons $a = 0.02 + 0.08\sigma$, $b = 0.25 - 0.05\sigma$, $c = -65$, and $d = 2$, where $\sigma \in (0, 1)$ is a random variable. Additionally, all neurons have $I_{\text{DC}} = 0$, except for the excitatory

neurons in population 1, which are submitted to a constant current of $I_{\text{DC}} = 25$ pA.

The synaptic transmissions are mediated by excitatory AMPA (A, related to $\alpha$-amino-3-hydroxy-5-methyl-4-isoxazolepropionic acid receptors) and fast inhibition GABAA (G, related to $\gamma$-aminobutyric acid). The presynaptic current is described as $I_{\text{syn}} = -g_{\text{syn}}r(v - V_{\text{syn}})$, where $V_A = 0$ mV and $V_G = -65$ mV. $g_{\text{syn}}$ is the maximal conductance, $g_A$ is for excitatory synapses, and $g_G$ is for inhibitory synapses. $r$ is the gating variable and follows a first-order kinetic dynamics: $\tau_{\text{syn}}dr/dt = -r + D\sum_j \delta(t - t_j)$, where $\tau_A = 5.26$ ms, $\tau_G = 5.60$ ms, and the summation over $j$ stands for the neighbor's presynaptic spikes at the previous time step $t_j$. $D$ is taken, without loss of generality, to be equal to 0.05. Also, all neurons are subject to an independent noisy spike train described by a Poisson distribution with rate $R$. The input mimics excitatory synapses from neurons that are not included in the populations. For population 1 we have employed $R = 3000$ Hz, and for population 2, $R = 2400$ Hz with the maximal conductance set to $g_A^{\text{Poisson}} = 0.6$ nS.

For the connectivity, each neuron, excitatory or inhibitory, receives 50 randomly chosen synapses from other neurons within the same population. Excitatory and inhibitory conductances are set to $g_A^1 = 3$ nS and $g_G^1 = 16$ nS for population 1 and $g_A^2 = 0.8$ nS and $g_G^2 = 16.4$ nS for population 2. For the connectivity between populations, each neuron in population 1 (2) receives 20 randomly chosen synapses from excitatory neurons from population 2 (1). The conductances are set to $g_A^{12} = 0.15$ nS and $g_A^{21} = 4$ nS, from 1 to 2 and from 2 to 1, respectively. For the simulations in Fig. 3 below, where feedback and feedforward strength connections were decreased or increased by 50%, we decreased or increased $g_A^{12}$ and $g_A^{21}$ simultaneously by the same amount.

It is worth mentioning that to adjust the rhythms at the gamma band we have modified the internal synaptic conductances $g_A^1$ and $g_G^1$ and the external constant current $I_{\text{DC}}$, but the effect of modifying other parameters such as the number of inhibitory neurons and the number of synapses could also be explored. The model was implemented in a C++ code and simulated using the Euler method, with a time step of $5 \times 10^{-2}$ ms. Our code is available from GitHub [20].

### B. Time series analysis in the frequency domain: Power, coherence, and Granger causality

To determine functional connectivity at the population level we analyzed the time series generated from the average membrane potential of excitatory neurons in each population: $V_X = \sum_{i=1}^{400} v_i$, where $v$, the cell's membrane potential, is given by Eq. (1) and $X$ stands for the population ($X = 1, 2$). Power, coherence, and Granger causality spectral analyses of our simulated time series were calculated using a methodology similar to that employed in Refs. [18,21] and the MVGC MATLAB toolbox [22]. The multivariate autoregressive (MVAR) modeling method employed here, which is based on the Wiener-Granger causality method, models the value of a stochastic process at current time $t$ in terms of its $p$ past values at times $t_1, \ldots, t_p$. The regression coefficients represent the predictable structure of the data, whereas the residuals

represent the unpredictable structure (see Refs. [22–24] for more details about the Granger causality).

To estimate the spectral analysis from the local field potential (LFP) time series, the MVAR requires the ensemble of single-trial time series to be treated as if it were produced from a zero-mean stochastic process. Therefore, we have analyzed the simulated time series of each population as if it were generated by 100 repetitions of 480 ms each (which is equivalent to 100 time series of 96 points with a sample rate of 200 Hz). It is also necessary to determine an optimal order for the MVAR model. For this purpose, we obtained the minimum of the Akaike information criterion [25] as a function of the model order (which we allowed to vary from 1 to 10; that is, we considered influences up to 50 ms in the past).

We calculated the spectral matrix elements $S_{XY}(f)$, with $X = 1, 2$ and $Y = 1, 2$, from which the coherence spectrum $C_{12}(f) = |S_{12}|/[S_{11}(f)S_{22}(f)]$ and the phase difference spectrum $\Phi_{lk}(f) = \tan^{-1}\{\mathrm{Im}[S_{lk}/\mathrm{Re}(S_{lk})]\}$ were calculated. A peak of $C_{12}(f)$ indicated synchronized oscillatory activity at the peak frequency $f_{\mathrm{peak}}$, with a time delay $\tau_{lk} = \phi_{lk}(f_{\mathrm{peak}})/(2\pi f_{\mathrm{peak}})$. The directional influence from population $X$ to population $Y$ was assessed via the Granger causality (GC) spectrum $G_{X \to Y}(f)$. We say that if the $p$ past values of $X$ do convey information about the future of $Y$ above and beyond all information contained in the past of $Y$, then $X$ Granger-causes $Y$. On the other hand, $X$ does not Granger-cause $Y$ if and only if $Y$, conditional on its own past, does not depend on the past of $X$. Since we are applying GC to only two neuronal populations we are not dealing with issues related to pairwise and conditioned Granger causality [26,27].

Since $G_{1 \to 2}(f)$ is calculated independently of $G_{2 \to 1}(f)$, the methodology can distinguish unidirectional and bidirectional influences for each frequency. To quantify the possible asymmetry between the influences from 1 to 2 and from 2 to 1, we can determine, for each frequency, the directed asymmetry index (DAI) between the two areas. The DAI was defined by Bastos *et al.* [11] to quantify the asymmetry between both directions of influence. Therefore, the DAI $A$ is computed as the normalized difference between spectral GC influences as in Ref. [11]:

$$A_{1 \to 2}(f) = \frac{G_{1 \to 2}(f) - G_{2 \to 1}(f)}{G_{1 \to 2}(f) + G_{2 \to 1}(f)}. \quad (3)$$

It is worth mentioning that GC has been applied over the population field potential that was estimated from the average value of the neuronal membrane potential, which is comparable to the LFP recorded in experiments [11]. Since the implementation of GC for spiking processes is not straightforward [28–30], we have employed a different methodology to estimate the directional flow of information between a pair of spike trains, as explained in the following section.

### C. Neuronal directional information estimation

To compute the DI from the spiking-neuron series we use the same methodology proposed by Tauste Campo *et al.* [17]. The method consists of estimating the directional flow of information between a pair of spike trains recorded simultaneously, which are assumed to be generated according to a Markovian process. Given a spike-train pair $(X^T, Y^T)$ of
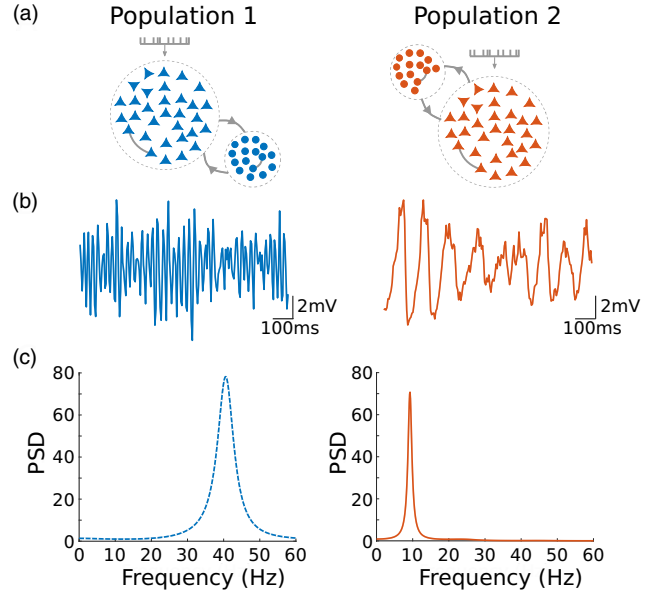


FIG. 1. Cortical motif circuits. (a) Schematic representation of two uncoupled cortical populations, 1 (left, blue) and 2 (right, orange), with excitatory and inhibitory neurons represented by triangles and circles, respectively. (b) Example of oscillatory activity for both populations, represented by the average membrane potential. (c) Power spectrum of the average membrane potential depicted in (b) (see text for details).

length $T$, time delay $D \geqslant 0$, and Markovian orders $M_1 > 0$ and $M_2 > 0$, the information-theoretic measure $I(D)$ quantifies the information that the past of $X$ at a delay $D$ has about the present of $Y$, i.e., $I(D) = I(X^{T-D} \to Y^T)$. The $I(D)$ significance is then determined via nonparametric testing of maximizing-delay statistics, which returns a statistic value and the maximizing delay. Finally, DI is defined as the spike-train pairs associated with significance estimators ($\alpha = 0.05$). In this context, feedforward, feedback, and bidirectional influences are defined when $X \to Y$, $X \leftarrow Y$, and $X \leftrightarrow Y$ are significant, respectively.

DI was estimated over a spike-train time series 10 s long from 100 randomly selected excitatory neurons of each population, i.e., 10 000 spike-train pairs. The spike train was binarized in 1 ms bins, and the time series was divided into 10 nonoverlapping time bins. Results are robust against changes in the bin size of the spike trains of up to 10 ms. DI was performed at time delays $D = 0, 2, 4, \ldots, 20$ with maximum memory $M_{1,2} = 2$, in accordance with Ref. [17]. The MATLAB code with directional information implementation is available from GitHub [31].

## III. RESULTS

To study the effect of unidirectional influence in one frequency band and the opposite direction of influence in another frequency band, we first simulate two uncoupled populations that could mimic, without loss of generality, areas V1 and V4 in the visual cortex. This will allows us, when we connect the two populations in the following sections, to identify population 1 as lower-order areas and population 2 as higher-order
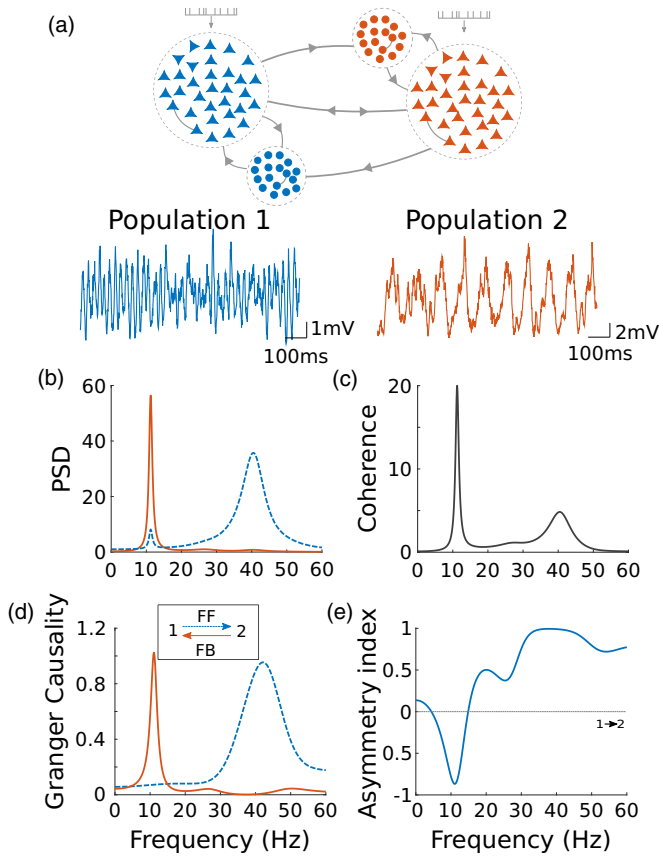
FIG. 2. Frequency-specific feedforward and feedback interactions. (a) Schematic representation of two cortical areas coupled in a bidirectional configuration and their average membrane potential. (b) Power spectral density of each population, 1 (blue, dashed) and 2 (orange, solid). (c) Spectral coherence (equivalent to the cross-spectral density) between the two areas. (d) Spectral Granger causality in both directions (feedforward: blue, dashed; feedback: orange, solid), showing that each of the peaks found in (c) corresponds to a particular direction of influence. (e) The directed influence asymmetry index (from population 1 to 2), or DAI profile of the functional connection, which is obtained by normalizing the difference between the two GC profiles [see Eq. (3)], can be used to characterize a directed functional connection between two cortical areas. Power, coherence, and Granger causality spectral analyses were calculated following a similar methodology employed in Refs. [18,21] and using the MVGC MATLAB toolbox [22].
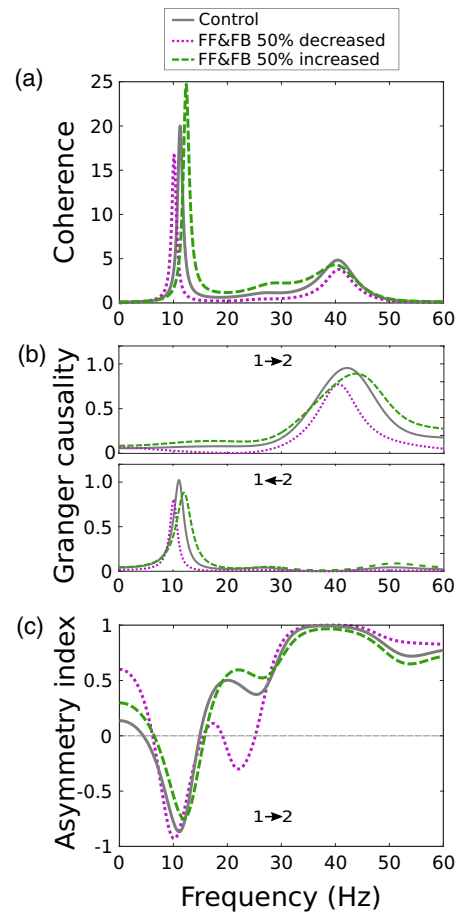


FIG. 3. Robustness of the bidirectional coupling in the parameter space. In the control case (gray, solid) the interareal synaptic conductances are set to $g_A^{12} = 0.15$ nS and $g_A^{21} = 4$ nS. For other cases the strength connections were decreased (purple, dotted) or increased (green, dashed) by 50%. (a) Spectral coherence. (b) Spectral Granger causality in feedforward (upper panel) and feedback (lower panel), showing that each of the peaks found in (c) corresponds to a particular direction of influence. (c) The directed influence asymmetry index (from population 1 to 2) profile of the functional connection.

areas in the hierarchical organization and reproduce the experimental results of feedforward and feedback interactions.

We adjust the parameters of each region to obtain population 1 oscillating in the gamma band (~40 Hz) and population 2 oscillating in the alpha band (~10 Hz) when isolated. In fact, several visual tasks have been related to an increase in the gamma activity of V1 [32,33]. Since the Granger causality from one network to the other is predominantly around the network oscillation frequency [34], we expect to obtain a causal flow from 1 to 2 at the gamma band and from 2 to 1 at the alpha band when we turn the connections on between the two networks in the following sections.

The important parameters to adjust the rhythms are the internal synaptic conductances and an external constant current applied to population 1 (see Sec. II for more details about the model). Figure 1 shows an illustrative example of the two populations, their oscillatory activity represented by the average membrane potential, and the power spectra associated with them.

### A. Frequency-dependent feedforward and feedback interactions

By connecting the two populations with chemical synapses in such a way that we know the structural connectivity [see Fig. 2(a)] we can measure their power spectrum as well as the synchronization and causal relations between their activity to infer the functional connectivity of our motif. In Fig. 2 we show the temporal evolution of the average membrane potential and its corresponding spectral analysis. First, the power spectrum [Fig. 2(b)] of each signal indicates that, due to the coupling, the two populations oscillate in both the gamma
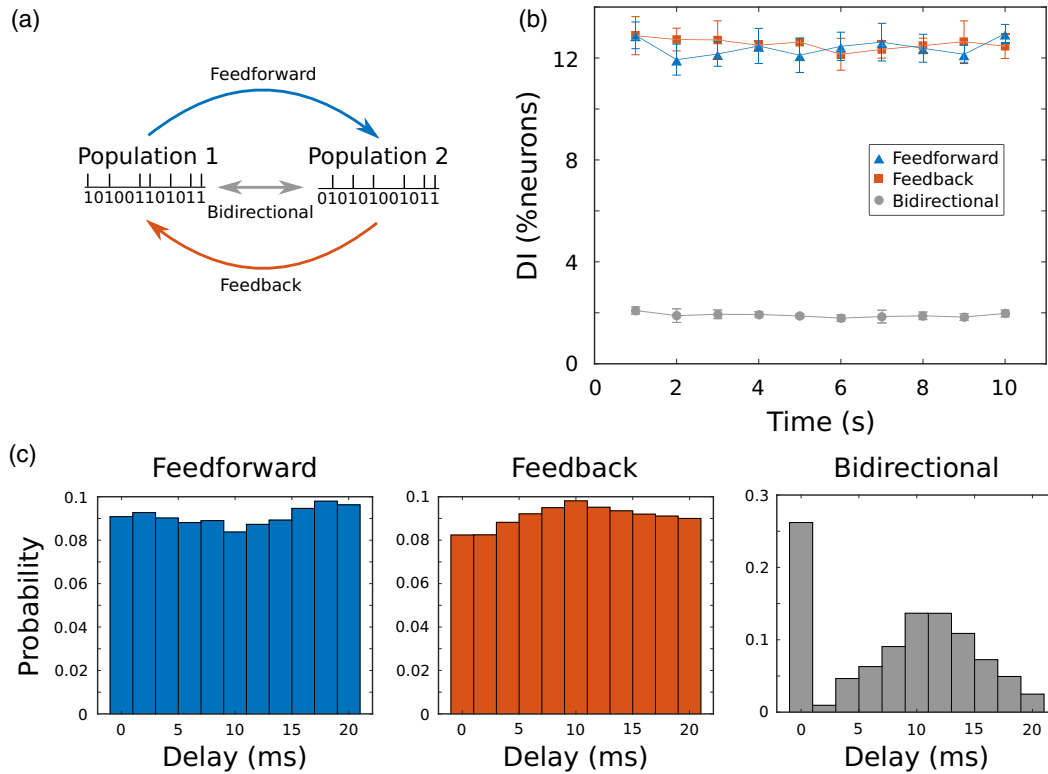
FIG. 4. Directional information between spike-train pairs. (a) Schematic representation of two spike trains from distinct populations: the directional information (DI) can be via feedforward (blue, population 1 → population 2), via feedback (orange, population 1 ← population 2), or bidirectional (gray, population 1 ↔ population 2). (b) Percentage of neuron pairs involved in feedforward, feedback, and bidirectional interactions assessed through DI (see Sec. II for details). (c) Delay distribution associated with the feedforward, feedback, and bidirectional interactions depicted in (b).

and alpha bands. Second, the coherence spectrum [Fig. 2(c)], characterizing the cross correlation in the frequency domain, shows that the activities of the two areas are synchronized predominantly around 10 and 40 Hz. Finally, the spectral Granger causality [Fig. 2(d)] profiles show that the statistical causal influence is from population 1 to population 2 (1 → 2) at the gamma band and the other way around (2 → 1) at the alpha band. This means that each of the peaks found in the coherence is related to a particular direction of influence.

The time delay $\tau_{lk}$ associated with each frequency peak in the coherence spectrum can be calculated from the phase difference spectrum (see Sec. II for more details). We have found that the time delay of the feedforward direction is $\tau_{12} = 3.6$ ms [related to $f_{\text{peak}} = 40.5$ Hz in Fig. 2(c)], whereas the time delay of the feedback interaction is $\tau_{21} = 5.3$ ms [related to $f_{\text{peak}} = 11.3$ Hz in Fig. 2(c)].

The DAI, which is obtained by normalizing the difference between the two GC profiles [see Eq. (3)], quantifies the asymmetry between the two directions of influence for each frequency [11]. The DAI profile in Fig. 2(e) corroborates that the directed functional connection between the two cortical areas is predominantly from 1 to 2 at the gamma band (30–60 Hz) and from 2 to 1 at the alpha band (7–13 Hz).

To verify whether the results are robust against model parameters, we modified the coupling parameters (between populations) in the simulation and reanalyzed the time series. In Fig. 3 we show that an increase or a decrease of 50% in the interareal synaptic conductances ($g_A^{12}$ and $g_A^{21}$) slightly shifts

the frequency of synchronization and influence but the overall results remain the same.

In order to test the statistical significance of the frequency shifts for each set of $g_A^{12}$ and $g_A^{21}$, we have extracted the peak frequency (for both coherence and GC) over 10 different realizations of our simulations. We have applied a Wilcoxon signed-rank test. Statistical significance was assessed at the population level by *post hoc* Wilcoxon signed-rank tests ($p < 0.05$). We have found that the mean frequencies of both alpha and gamma peaks increase (decrease) for an increase (decrease) of 50% in the interareal synaptic conductances when compared to the control case. We have obtained $p < 0.02$ for all comparisons.

**B. Feedforward and feedback influences at the neuronal scale**

As suggested by Bastos *et al.* [11], future experimental studies might test causality influences directly with simultaneous multiarea multilayer recordings of the LFP and spikes. Therefore, modeling the observed phenomena with a spiking-neuron network allows us to investigate specific properties of the spiking trains which could be compared in the future with similar experimental data. This simultaneous investigation of the LFP and spike would not be possible in a firing rate model.

We address the question of causal relation at the neuronal level by using a nonparametric directed information-theoretic measure [17,35]. DI allows the estimation of spiking direct influences from one population to another [Fig. 4(a)]. By

analyzing the interaction of 10 000 neuron pairs (100 neurons from population 1 with another 100 neurons from population 2; see Sec. II for details), we can estimate the percentage of neurons from population 1 that influence the neurons from population 2 (and vice versa) through feedforward (feedback) interactions. Moreover, we can quantify what percentage of these connections are bidirectional. In our population model, by estimating DI in 1 s long nonoverlapping time windows over 10 s long time series (see Sec. II for details), we obtained that both feedforward and feedback interactions are mediated by approximately the same number of neuron pairs, ~12% [Fig. 4(b)]. For bidirectional communication there are fewer neurons involved, ~2% [Fig. 4(b)].

To measure the communication delay through which neurons interact, we estimated delayed versions of the directed information-theoretic measure in both directions at short time delays $D = 0, 2, 4, \ldots, 20$ ms. The probability of finding an interaction for each delay is shown in Fig. 4(c). For feedforward and feedback interactions there is no preferred delay of communication [Fig. 4(c), left and middle], while for the bidirectional case the interaction occurs mostly at zero lag, followed by a less pronounced peak at around 10 to 12 ms [Fig. 4(c), right]. It is worth mentioning that these communication delays at the neuronal level are calculated at the time domain and not at a specific frequency. Therefore, they are different from the time delays $\tau_{lk}$ associated with the oscillatory activity in each frequency band at the populational scale.

## IV. CONCLUDING REMARKS

To summarize, we have shown that a simple but biophysically plausible model of two bidirectionally connected spiking-neuronal populations can present unidirectional Granger causality in the gamma frequency band and the opposite direction of causal flow in the alpha frequency band. Our model qualitatively reproduces experimental results verified with electrocorticograms in macaques and magnetoencephalograms in humans of feedforward and feedback influences through distinct frequency bands [11,12]. Therefore, our results are a verification *in silico* using a network model of spiking neurons of such a specific phenomenon

related to cortical synchronization which was previously reported *in vivo* in primates. In particular, there are two advantages to use spiking-neuron models: (i) investigating detailed mechanisms underlying the phenomena such as neuronal variability, heterogeneity, homeostasis, and synaptic plasticity within each population, and (ii) analyzing statistical properties of neuronal spiking series which could also be investigated in experimental setups.

Our results are a first step to explore more realistic and detailed spiking-neuron networks, including details about the different cortical layers [16,36]. It would be possible to use our model to explore a large-scale network with many cortical areas in order to explore hierarchic properties between visual regions, similar to what was done by Mejias *et al.* [13] with a firing rate model for each cortical layer. Such further steps would allow us to better compare the spiking-neuron population model and the experimental results reported in visual areas [11,12].

Furthermore, our findings open avenues to explore the role of phase diversity in the computational properties of brain signals, a subject that has gained the attention of the neuroscience community in recent years [37,38]. In light of anticipated synchronization ideas [18,39–42] it is possible to explore the mechanisms underlying the phase relation between the two populations in each frequency band both experimentally and numerically.

[1] D. J. Felleman and D. C. Van Essen, Cereb. Cortex **1**, 1 (1991).

[2] N. T. Markov, J. Vezoli, P. Chameau, A. Falchier, R. Quilodran, C. Huissoud, C. Lamy, P. Misery, P. Giroud, S. Ullman *et al.*, J. Comp. Neurol. **522**, 225 (2014).

[3] M. I. Posner, C. R. Snyder, and B. J. Davidson, J. Exp. Psychol.: General **109**, 160 (1980).

[4] J. Moran and R. Desimone, Science **229**, 782 (1985).

[5] E. A. Buffalo, P. Fries, R. Landman, T. J. Buschman, and R. Desimone, Proc. Natl. Acad. Sci. U.S.A. **108**, 11262 (2011).

[6] M. J. Roberts, E. Lowet, N. M. Brunet, M. Ter Wal, P. Tiesinga, P. Fries, and P. De Weerd, Neuron **78**, 523 (2013).

[7] D. Xing, C.-I. Yeh, S. Burns, and R. M. Shapley, Proc. Natl. Acad. Sci. U.S.A. **109**, 13871 (2012).

[8] T. Van Kerkoerle, M. W. Self, B. Dagnino, M.-A. Gariel-Mathis, J. Poort, C. Van Der Togt, and P. R. Roelfsema, Proc. Natl. Acad. Sci. U.S.A. **111**, 14332 (2014).

[9] J. H. Lee, M. A. Whittington, and N. J. Kopell, PLoS Comput. Biol. **9**, e1003164 (2013).

[10] P. Fries, Trends Cognit. Sci. **9**, 474 (2005).

[11] A. M. Bastos, J. Vezoli, C. A. Bosman, J.-M. Schoffelen, R. Oostenveld, J. R. Dowdall, P. De Weerd, H. Kennedy, and P. Fries, Neuron **85**, 390 (2015).

[12] G. Michalareas, J. Vezoli, S. Van Pelt, J.-M. Schoffelen, H. Kennedy, and P. Fries, Neuron **89**, 384 (2016).

[13] J. F. Mejias, J. D. Murray, H. Kennedy, and X.-J. Wang, Sci. Adv. **2**, e1601335 (2016).

[14] R. Baravalle and F. Montani, Phys. Rev. E **103**, 042308 (2021).

[15] R. Zeraati, V. Priesemann, and A. Levina, Front. Phys. **9**, 103 (2021).

[16] J. H. Lee, M. A. Whittington, and N. J. Kopell, J. Neurosci. **35**, 15000 (2015).

[17] A. Tauste Campo, Y. Vázquez, M. Álvarez, A. Zainos, R. Rossi-Pool, G. Deco, and R. Romo, Proc. Natl. Acad. Sci. U.S.A. **116**, 7513 (2019).

[18] F. S. Matias, L. L. Gollo, P. V. Carelli, S. L. Bressler, M. Copelli, and C. R. Mirasso, NeuroImage **99**, 411 (2014).

[19] E. Izhikevich, IEEE Trans. Neural Networks **14**, 1569 (2003).

[20] https://github.com/ldallap/BidirectionalGrangerModel.

[21] A. Brovelli, M. Ding, A. Ledberg, Y. Chen, R. Nakamura, and S. L. Bressler, Proc. Natl. Acad. Sci. U.S.A. **101**, 9849 (2004).

[22] L. Barnett and A. K. Seth, J. Neurosci. Methods **223**, 50 (2014).

[23] C. W. J. Granger, Econometrica **37**, 424 (1969).

[24] V. J. López-Madrona, F. S. Matias, C. R. Mirasso, S. Canals, and E. Pereda, Sci. Rep. **9**, 1 (2019).

[25] H. Akaike, IEEE Trans. Autom. Control **19**, 716 (1974).

[26] S. Stramaglia, T. Scagliarini, B. C. Daniels, and D. Marinazzo, Front. Physiol. **11**, 1784 (2021).

[27] S. Stramaglia, J. M. Cortes, and D. Marinazzo, New J. Phys. **16**, 105003 (2014).

[28] D. P. Shorten, R. E. Spinney, and J. T. Lizier, PLoS Comput. Biol. **17**, e1008054 (2021).

[29] R. E. Spinney, M. Prokopenko, and J. T. Lizier, Phys. Rev. E **95**, 032319 (2017).

[30] G. Mijatovic, Y. Antonacci, T. L. Turukalo, L. Minati, and L. Faes, IEEE Trans. Biomed. Eng. (2021).

[31] https://github.com/AdTau/DI-Inference.

[32] J. A. Henrie and R. Shapley, J. Neurophysiol. **94**, 479 (2005).

[33] X. Jia, D. Xing, and A. Kohn, J. Neurosci. **33**, 17 (2013).

[34] L. Faes, S. Stramaglia, and D. Marinazzo, F1000Research **6**, 1710 (2017).

[35] A Tauste Campo, Comput. Struct. Biotechnol. J. **18**, 2699 (2020).

[36] T. C. Potjans and M. Diesmann, Cereb. Cortex **24**, 785 (2014).

[37] E. Maris, T. Womelsdorf, R. Desimone, and P. Fries, Neuroimage **74**, 99 (2013).

[38] E. Maris, P. Fries, and F. van Ede, Trends Neurosci. **39**, 86 (2016).

[39] H. U. Voss, Phys. Rev. E **61**, 5115 (2000).

[40] F. S. Matias, P. V. Carelli, C. R. Mirasso, and M. Copelli, Phys. Rev. E **84**, 021922 (2011).

[41] F. S. Matias, L. L. Gollo, P. V. Carelli, C. R. Mirasso, and M. Copelli, Phys. Rev. E **94**, 042411 (2016).

[42] L. Dalla Porta, F. S. Matias, A. J. dos Santos, A. Alonso, P. V. Carelli, M. Copelli, and C. R. Mirasso, Front. Syst. Neurosci. **13**, 41 (2019).